

New Planetary Nebulae in the Galactic Bulge region with $l > 0^\circ$ - I. Discovery method and first results

P. Boumis¹*†, E. V. Paleologou¹, F. Mavromatakis¹ and J. Papamastorakis^{1,2}

¹Department of Physics, University of Crete, P.O. Box 2208, GR-710 03 Heraklion, Crete, Greece.

²Foundation for Research and Technology-Hellas, P.O. Box 1527, GR-711 10 Heraklion, Crete, Greece.

Received 2002 April 5. Accepted 2002 November 1

ABSTRACT

We present the first results of an [O III] 5007 Å interference filter survey for Planetary Nebulae (PNe) in the Galactic bulge. Covering (at first) the 66 per cent of the survey area, we detected a total of 90 objects, including 25 new PNe, 57 known PNe and 8 known PNe candidates. Deep H α +[N II] CCD images have been obtained as well as low resolution spectra for the newly discovered PNe. Their spectral signature suggests that the detected emission originates from a photoionized nebula. In addition, absolute line fluxes have been measured and the electron densities are given. Accurate optical positions and optical diameters were also determined.

Key words: ISM: planetary nebulae: general - Galaxy: bulge - surveys

1 INTRODUCTION

The Galactic Planetary Nebulae are of great interest because of their important role to the chemical enrichment history of the interstellar medium as well as in the star formation history and evolution of our Galaxy (Beaulieu et al. 2000 and references therein). The study of PNe offers the opportunity to determine basic physical parameters (like morphology, kinematics, abundances, distances, masses etc.), which will help to test theoretical models and understand more about the bulge dynamics (see sect. 2). The distance determinations of PNe in the Galactic bulge suggest distances at ~ 8 kpc (7.8 kpc; Feast 1987, 8.3 ± 2.6 kpc; Schneider & Buckley 1996). The Galactic bulge extends over a region of galactic longitude $l \simeq \pm 15^\circ$ and galactic latitude $b \simeq \pm 10^\circ$ (dimensions ~ 2 kpc toward and ~ 1.5 kpc perpendicular the Galactic plane, respectively - Weiland et al. 1993). In total, the bulge contains about 10^{11} stars of Population II as well as gas ($\sim 10^6 M_\odot$) and dust (mass ~ 100 times less than the mass of the gas - Morison & Harding 1993). It is generally accepted that a large number of PNe exists in the Galactic bulge, but because of the excessive interstellar extinction, only a small number of them (less than 500) have been discovered (Köppen & Vergely 1998; Parker et al. 2001b). According to Acker et al. (1992a) and Zijlstra &

Pottasch (1991), the total number of PNe in the Galaxy is estimated between 15,000 to 30,000. Approximately, 3,400 PNe have been discovered up to date, meaning that only a small number of all PNe have been detected. In particular, Acker et al. (1992b, 1996) report 2204 objects which have been classified as true, probable and possible PNe. Most of them were found through surveys in different wavebands (optical, radio, infrared - Moreno et al. 1988; Pottasch et al. 1988; Ratag 1990; van de Steene 1995, etc.). Kohoutek (2001) presented 169 additional new PNe which were discovered through different surveys between the years 1995-1999, while Cappellaro et al. (2001) published a catalogue of 16 new PNe discovered towards the galactic center. In a very recent catalogue, Parker et al. (2001b) presented more than 900 new and candidate PNe which were discovered during the AAO/UKST H α survey of PNe in the Galactic plane. Note that not all surveys utilized narrow band imagery to identify candidate PNe (e.g. Lauberts 1982).

The task of determining the wavelength band suitable for a search of new PNe in the bulges is under debate. The interstellar extinction being higher in the direction of the bulge, reduces the effectiveness of the optical surveys. For this reason, radio continuum and far-infrared surveys were made in regions with high extinction, resulting to new PNe discoveries. On the other hand, as Beaulieu, Dopita & Freeman (1999) noted long waveband surveys work well only with dusty (young) PNe while the low-density (old) PNe are undetectable by IRAS. Furthermore, it is well known that most PNe emit strongly in the H α and [O III] 5007 Å lines, and that the latter is affected more

* e-mail: ptb@astro.noa.gr

† Present address: Institute of Astronomy & Astrophysics, National Observatory of Athens, I. Metaxa & V. Paulou, GR-152 36 P. Penteli, Athens, Greece

by interstellar extinction than $\text{H}\alpha$. Moreover, $[\text{O III}]$ bright PNe display $\text{H}\alpha/[\text{O III}] 5007 \text{ \AA} < 1$ and mainly the low-density PNe. Recent high resolution spectrophotometric observations (Cuisinier et al. 2000; Escudero & Costa 2001) determined the abundances of known PNe in the Galactic bulge. Using these results, a comparison between the $\text{H}\alpha$ and $[\text{O III}]$ line intensities shows that 40 per cent of them display $\text{H}\alpha/[\text{O III}] 5007 \text{ \AA} < 1$.

The right combination of the telescope size and the CCD camera, depending on the distance to search, can provide a useful tool for the detection of new PNe (Ciardullo et al. 1989; Jacoby et al. 1990; Feldmeier, Ciardullo & Jacoby 1997 and references therein). Therefore, we decided to performed survey observations of the Galactic bulge using the 0.3 m telescope of a wide field of view (combined with a highly efficient CCD camera) and a narrow $[\text{O III}] 5007 \text{ \AA}$ filter. The $[\text{O III}] 5007 \text{ \AA}$ filter (like any other emission line filter) may not be the best choice for the detection of new PNe but note that a significant number of PNe are characterized by strong $[\text{O III}] 5007 \text{ \AA}$ emission relative to $\text{H}\alpha$. We must note that a PN discovery has already been done in the past using this configuration (Xilouris et al. 1994).

Informations concerning the importance of PNe in the bulge are given in sect. 2, the $[\text{O III}]$ survey (observations and analysis) are given in sect. 3, while in sect. 4 we present follow-up observations (CCD imaging and spectroscopy) of the newly discovered PNe. In addition, flux measurements, diameter determination, accurate positions and other physical properties for the new PNe are given in sect. 5. We must note that this paper is the first of a sequence, where we will present in detail imaging and spectrophotometric results for all the new PNe discovered in our survey, as well as fitted models to describe their physical parameters. In particular, images and spectra for the new PNe found in the remaining fields will be presented, while flux calibrated images for most of the new PNe will be used in PNe models (e.g. van Hoof & van de Steene 1999) in order to determine their physical parameters (like abundances, distances etc.).

2 PLANETARY NEBULAE AS TRACERS OF THE GALACTIC BULGE

Many tracers have been used in the past to study the Galactic bulge. In particular, the OH/IR stars (e.g. Sevenster 1999), the M giant stars (e.g. Minniti et al. 1996a; Minniti 1996b), the Miras and other LPVs (Whitelock 1994), the carbon stars (Whitelock 1993), the K giants stars (e.g. Minniti et al. 1995; Minniti 1996b), the RR Lyrae stars (Walker & Terndrup 1991) and the PNe (Kinman, Feast & Lasker 1988; Durand, Acker & Zilstra 1998; Beaulieu et al. 2000). The first three (OH/IR, Miras and M giant stars) are biased toward the metal-rich population. The carbon stars are also an indication of metal-rich population but they are not very numerous in the Galaxy. The K giant stars have been used a lot as tracers since they can be found at all metallicities but they are biased because of their faintness. The RR Lyrae stars represent the metal-poor tail of the bulge metallicity distribution and they are also faint.

On the other hand, PNe are not biased toward the metal-rich population (Hui et al. 1993). They originate from intermediate and low initial mass stars and therefore consti-

tute a relatively old population. The He and N abundances are modified along the stellar evolution of the progenitor and can be related to their masses and age. Their optical spectrum is dominated by strong emission lines (like $\text{H}\alpha$ and $[\text{O III}]$) allowing accurate velocity measurements. Up to now, their distances are not well defined since it is difficult to determine their absolute diameter which is necessary for distance calculation (e.g. Schneider & Buckley 1996). However, Gathier et al. (1983) estimated that a large number of PNe with small diameters ($\leq 20''$) belong to the Galactic bulge according their angular diameter, spatial distribution and radial velocities measurements. Taking into account all the parameters discussed in this section, the Galactic bulge PNe appear as a very important tool in order to study the dynamics and kinematics of the Galactic bulge.

3 THE $[\text{O III}] 5007 \text{ \AA}$ SURVEY

3.1 Observations

The observations reported here were made with the 0.3 m Schmidt-Cassegrain (f/3.2) telescope at Skinakas Observatory in Crete, Greece. An $[\text{O III}] 5007 \text{ \AA}$ interference filter with an 28 \AA bandwidth was used in combination with a Thomson CCD (1024 \times 1024, 19 \times 19 μm^2 pixels). This configuration results in a scale of 4''.12 pixel $^{-1}$ and a field of view of 71' \times 71' on the sky. In our survey we observed the regions $10^\circ < l < 20^\circ$, $-10^\circ < b < -3^\circ$ and $0^\circ < l < 20^\circ$, $3^\circ < b < 10^\circ$ (named Field A and Field B, respectively in Fig. 1). The reasons to do this was (a) the site of the Observatory which allows us to observe down to -25° declination and (b) the $[\text{O III}] 5007 \text{ \AA}$ emission line which is heavily absorbed between $-3^\circ < b < 3^\circ$. In our survey, we tend to discover planetary nebulae which (1) characterized by strong $[\text{O III}] 5007 \text{ \AA}$ emission, (2) are slightly extended because of our spatial resolution (3) are point-like with signal to noise greater than 4 (4) do not have declination below -25° and (5) are observed only during dark time periods to avoid the moonlight scattering effect to the $[\text{O III}] 5007 \text{ \AA}$ line. We must note that the area of the Galactic Bulge was also covered by the AAO/UKST $\text{H}\alpha$ survey (Parker et al. 2001a – in fact they have covered the total area of the southern Galactic plane). In Fig. 1 the filled rectangles represent the observed fields. We covered at first a region of 66 per cent of the proposed grid (116 fields out of 179) because of the availability of the telescope with respect to the time needed to complete the survey. The observational details are given in Table 1. During the 2001 observing season we observed the remaining 62 fields (Boumis et al. 2003 - Paper II). All the objects were observed between airmass 1.4 to 2.0 in similar observing and seeing conditions.

Two exposures in $[\text{O III}] 5007 \text{ \AA}$ of 1200 s and three exposures in the continuum of 180 s were taken to make sure that any cosmic ray hits will be identified and removed successfully (see section 3.2 for the image processing details). Two different continuum filters were used, dependent on their availability. Details about the filters are given in Table 2.

Table 2. Filters used for the Imaging Survey

Filter	Central wavelength (Å)	FWHM (Å)	Type	Manufacturer
[O III] 5007 Å	5005	28	Interference	Spectrofilm
Continuum	5470	230	Strömgren-y	Custom Scientific
Continuum	6096	134	Interference	Spectrofilm

Table 1. Observational details for the [O III] 5007 Å Imaging Survey

Date	Number of observing nights	Number of clear nights
2000 May 6-7	2	2
2000 May 25-31	7	3
2000 Jun 25-29	5	5
2000 Jul 1-7	7	7
2000 Jul 24-27	4	4
2000 Jul 31-Aug 3	5	5
2000 Aug 24-Aug 28	5	5
2000 Aug 30-Sep 04	6	6

3.2 Analysis

Standard IRAF, MIDAS and STARLINK routines were used for the reduction of the data. The analysis was performed by using three different packages since different tasks were easier and more accurate to perform in certain packages than in others. Individual images were bias subtracted and flat-field corrected through observations of the twilight sky. In particular, approximately 15 bias frames and 11 twilight flat-field frames (in each filter) were obtained each night and the master bias and flat-field frames (for each filter) were used in the image processing. The sky background has also been subtracted from each individual frame. No dark frames were used, since the dark current was negligible for the exposure time used.

3.2.1 Selection of the PNe candidates

It is difficult to detect faint emission sources in a very dense star field as in the Galactic bulge. Therefore, special techniques must be followed to attack this problem. It is well known that for the detection of faint emission line sources - like the PNe in our case - a narrow-band filter (i.e. [OIII]) should be used in combination with a wider-band filter (continuum) where no significant emission lines exist and only the field stars appear. The correct scaling and subtraction of the two images will suppress the field stars and only the [OIII] emitters and possible cosmic rays will still be visible.

Our detection method (Boumis & Papamastorakis 2002) is similar but not the same to that followed in the Galactic bulge by Beaulieu et al. (1999). Their idea was to combine two $H\alpha$ frames and then divide the summed image by the continuum image for each field. Here, instead of division, we identify the PNe candidates by following another approach. In particular, after calculating the correct scaling between the stars from the [OIII] and the continuum images (the three continuum images of each field were combined to produce a master continuum), we subtracted from each

of the two [OIII] images the corresponding master continuum image for each field. In order to do the correct scaling (match the total star signal above the sky in both images), we chose a box of a specific number of pixels where non saturated stars were included. The continuum images were multiplied by a factor f (similar to that given by Beaulieu et al. 1999) and then their total star signal was the same as for the [OIII] images. The initial PNe identification was performed by “blinking” each continuum subtracted [OIII] frame and the corresponding continuum. Given the angular size of ~ 4 arcsec of a CCD pixel, the PNe candidates at the bulge appeared as slightly extended (or sometimes point-like) sources on the [OIII] images, but were absent in the continuum. As mentioned above, the new sources could be PNe candidates or cosmic rays. To make sure that no cosmic rays were included among the candidates, we checked visually each individual [OIII] frame for each field. Objects that appeared bright in one frame but were absent in the other, were considered as cosmic ray hits because a real emission source should be present in both [OIII] images. Another limitation was that all point-like objects have a signal to noise greater than 4 according to their count measurements since the survey images are not flux calibrated. We must note that we have tried to follow Beaulieu et al. (1999) method and the two [OIII] images of each field were combined before subtraction in order to increase the signal to noise ratio. However, the problem of removing correctly the cosmic rays still remained and we decided to perform the blinking technique between the two continuum subtracted [OIII] images and the corresponding master continuum image. After a very detailed and systematic visual investigation of 116 fields, we identified 90 objects. The procedure of how the PNe candidates looked like through the different steps can be seen in Fig. 2, where there are examples of images ($20'$ on both sides each) for three different objects which show our survey’s typical discoveries. The first set of images (a) is a known PN which was found and presented for comparison reasons; the other two sets (b) and (c) are new discoveries. Note that the remaining black dots in the last image of each set (except the PNe) are cosmic rays which were not removed by the continuum subtraction but clearly identified since they do not appear in both the continuum subtracted [O III] images.

3.2.2 Preliminary Astrometry & Survey Results

After identifying the PNe candidates, the next step was to perform an astrometric solution for all images containing one or more candidates. In order to calculate the equatorial (and galactic) coordinates of the PNe candidates, we used the Hubble Space Telescope (HST) Guide Star Catalog (Lasker, Russel & Jenkner 1999) and IRAF routines

(Image package). Typical rms error in each frame was found to be $\sim 1''.3$ using the task “ccmap” in the Image package of IRAF. The 90 objects were then checked in order to identify the already known PNe. For that purpose we used any up-to-date published catalogue related to planetary nebulae. A list of all catalogues used is given in Table 3. The search showed that from the 90 objects found in our survey, the 57 are known PNe, 8 are known PNe candidates and 25 are new PNe candidates. Note that independently from our search, Parker et al. (2001b) presented a new catalogue of GBPNe where 17 of our new PNe are included as new and candidate PNe (see Table 4). In order to make sure that all catalogued PNe which fall in our fields were detected, we performed a second search and found that 16 known PNe and 14 known PNe candidates are not included in our detections. However, knowing their position a re-examination showed that most of the “missed” known PNe and PNe candidates do appear in our survey frames as very faint point sources due to their small angular size and their very low signal to noise ratio ($\sim 1\sigma$). The 8 known PNe candidates which have been confirmed in our survey (in galactic coordinates) are: 003.9+02.7, 004.4+06.4, 006.7+03.4, 007.8-03.8, 008.3+03.7, 009.3-06.5, 019.0-04.2 and 019.7-08.2. Note, that all the above PNe and PN candidates are listed in the catalogues given in Table 3.

3.2.3 Search in other wavelengths

We performed a search in the IRAS Point Source Catalog (1988) in order to check for possible presence of dust to the new PNe candidates and found matches for 9 of our new objects (see Table 4 for details concerning their F_{12} , F_{25} , F_{60} , F_{100} fluxes and their flux quality density). Taking into account the fact that the flux quality density for most of them was 1 (1 is the upper detection limit, whereas 3 is a good quality flux density), a reasonable number of them satisfy the standard criteria ($F_{12}/F_{25} \leq 0.35$ and $F_{25}/F_{60} \geq 0.3$ – Pottasch et al. 1988; van de Steene 1995) used to accept a new object as a probable PN. Note that a cross-check for our new PNe was also performed both with the 2MASS Point Source Catalog (2000), the MSX infrared astrometric Catalog (Egan et al. 1999) and radio known PNe (found in the catalogues given in Table 3) in order to find any PNe counterparts but the results proved negative most likely due to the low sensitivity limit of these surveys. Thus, radio pointed observations at selected locations would be needed.

4 THE 1.3 METER TELESCOPE OBSERVATIONS

4.1 Imaging

Optical images of the new PNe candidates were also obtained with the 1.3 m (f/7.7) Ritchey-Cretien telescope at Skinakas Observatory during 2001 in May 27–29, June 29–30 and August 10–11 using an $H\alpha+[N\,II]$ interference filter (75Å bandwidth). The detector was a 1024×1024 (with $24 \times 24 \mu\text{m}^2$ pixels) SITe CCD with a field of view of $8''.5 \times 8''.5$ and an image scale of $0''.5 \text{ pixel}^{-1}$. One exposure in the $H\alpha+[N\,II]$ of 1800 s and two exposures in the continuum

of 180 s were taken. All new PNe candidates observed with this configuration can be seen in Fig. 4. Note that they are at the centre of each image and an arrow points to their exact position. The image size is $150''$ on both sides. North is at the top and east to the left. It should be noticed that taking into account the limited telescope time available, the follow-up observations were performed in $H\alpha+[N\,II]$ in order to study the morphology of the PNe and also measure their angular extent.

After finding the PNe candidates, we performed again an astrometric solution for all images, using the method presented in section 3.2.2. The coordinates for the PNe candidates were now calculated with better accuracy, due to the 8 times better resolution of this configuration. Typical rms error in each frame was found to be $\sim 0''.3$. Hence, the coordinates of all the newly discovered PNe candidates are given in Table 4.

4.2 Spectroscopy

Low dispersion spectra were obtained with the 1.3 m telescope at Skinakas Observatory during 2001 in June 24–28, July 16–17, 23–25 and August 12, 20–25. A 1300 line mm^{-1} grating was used in conjunction with a 2000×800 SITe CCD ($15 \times 15 \mu\text{m}^2$ pixels) which resulted in a dispersion of 1 \AA pixel^{-1} and covers the range of $4750\text{\AA} - 6815\text{\AA}$. The slit width was $7''.7$ and it was oriented in the south–north direction, while the slit length was $7''.9$. The exposure time of the individual spectra ranges from 2400 to 3600 s depending on the observing window of each object. Two spectra of the same object were obtained whenever possible and in this case the S/N weighted average line flux values are given. The spectrophotometric standard stars HR5501, HR7596, HR9087, HR718, and HR7950 (Hamuy et al. 1992; 1994) were observed in order to calibrate the spectra of the new PNe candidates. The low resolution spectra were taken on the relatively bright optical part of each PN candidate. Some typical spectra of our new PNe can be seen in Fig. 7. In Table 5, we present their line fluxes corrected for atmospheric extinction and interstellar reddening, using the scale of $F(H\beta)=100$. Interstellar reddening was derived from the $H\alpha/H\beta$ ratio (Osterbrock 1989), using the interstellar extinction law by Fitzpatrick (1999) and $R_v = 3.1$ for all objects. Therefore, the interstellar extinction $c(H\beta)$ can be derived by using the relationship

$$c(H\beta) = \frac{1}{0.348} \log \frac{F(H\alpha)/F(H\beta)}{2.85} \quad (1)$$

where, 0.348 is the relative logarithmic extinction coefficient for $H\beta/H\alpha$ and 2.85 the theoretical value of $F(H\alpha)/F(H\beta)$. The observational reddening in magnitude E_{B-V} was also calculated using the relationship (Seaton 1979)

$$c(H\beta) = 0.4 \cdot X_\beta \cdot E_{B-V} \quad (2)$$

where the extinction parameter $X_\beta = 3.615$ (Fitzpatrick 1999). The 1σ error of the extinction $c(H\beta)$ and E_{B-V} was calculated through standard error propagation of equations (1) and (2). Because of the high interstellar extinction in the direction of the bulge a second estimation of E_{B-V} was made using the SFD code (Schlegel, Finkbeiner & Davis 1998) which uses infrared maps to estimate Galactic extinction.

Table 3. A list with all the planetary nebulae catalogues used. Note that the Strasbourg-ESO Catalogue was used as a reference, because it was the most complete catalogue up to 1992. Ratag's thesis was the only exception as it was published before 1992 but it was not included in the above catalogue.

No	Catalogue	Reference
1	A Study of GBPNe	Ratag 1990
2	Strasbourg-ESO Catalogue of GPNe (Part I, II)	Acker et al. 1992
3	Obscured PNe	van de Steene 1995
4	First Supplement to the Strasbourg-ESO Catalogue of GPNe	Acker et al. 1996
5	IAC Morphological Catalog of Northern GPNe	Manchado et al. 1996
6	Catalogue of GPNe (1990-1994)	Kohoutek 1997
7	Innsbruck Data Base of GPNe	Kimeswenger, Kienel & Widauer 1997
8	Kinematics of 867 GPNe	Durand, Acker & Zijlstra 1998
9	Infrared PN in the NRAO VLA Sky Survey	Condon, Kaplan & Terzian 1999
10	A Survey of PNe in the Southern Galactic Bulge	Beaulieu et al. 1999
11	Version 2000 of the Catalogue of GPNe	Kohoutek 2001
12	Radio Observations of New GBPNe	van de Steene et al. 2001
13	Optical Coordinates of Southern PNe	Kimeswenger 2001
14	New PNe towards the galactic center	Cappellaro et al. 2001
15	The Edinburgh/AAO/Strasbourg Catalogue of GPNe	Parker et al. 2001b

Table 4. Newly discovered PNe.

Object	PN G (lll.l \pm bb.b)	RA (J2000)	Dec (J2000)	IRAS source	F_{12} (Jy)	F_{25} (Jy)	F_{60} (Jy)	F_{100} (Jy)	F_{Quality} (12,25,60,100 μm)	Ref ^a
PTB1	003.5+02.7	17 43 39.2	-24 31 53.0	17405-2430	3.35	2.88	2.60	18.2	1,1,3,1	1a
PTB2	004.1+07.8	17 26 12.2	-21 17 53.0							1a
PTB3	004.6+06.1	17 33 33.0	-21 51 23.2							1b
PTB4	005.4+04.0	17 42 54.7	-22 14 16.3							1a
PTB5	005.7+04.5	17 41 38.7	-21 44 32.2	17386-2143	2.56	0.876	1.08	10.7	1,1,3,1	
PTB6	006.1+03.9	17 45 06.5	-21 41 55.1							1a
PTB7	007.1+07.4	17 34 30.2	-19 01 01.1							1b
PTB8	007.2+03.4	17 49 13.7	-21 01 42.9	17462-2100	1.19	0.712	1.41	12.1	1,3,3,1	1a
PTB9	007.2+04.9	17 43 34.0	-20 13 55.7							1b
PTB10	007.3+03.5	17 49 26.7	-20 54 31.1							
PTB11	007.4-03.0	18 13 40.2	-23 57 38.5							
PTB12	007.9+04.3	17 47 15.6	-19 57 27.6							1b
PTB13	008.8+03.8	17 51 08.7	-19 25 46.6							2
PTB14	009.4+03.9	17 52 17.8	-18 52 02.4							
PTB15	011.5+03.7	17 57 05.6	-17 11 09.7	17541-1710	0.305	0.78	1.28	13.1	1,3,3,1	1a
PTB16	012.0+07.4	17 45 07.5	-14 53 23.4							1a
PTB17	012.5+04.3	17 57 10.5	-15 56 17.3							1a,2
PTB18	013.4+08.8	17 42 58.0	-12 56 46.9							1a
PTB19	014.0+04.8	17 58 26.0	-14 25 25.1	17555-1425	0.29	0.502	1.58	7.68	1,3,3,1	
PTB20	016.1+07.7	17 52 15.0	-11 10 35.6	17494-1109	0.269	0.466	0.71	3.49	1,3,3,1	
PTB21	016.6+07.0	17 55 53.3	-11 05 41.7	17529-1103	1.03	0.459	0.529	4.16	3,1,1,1	
PTB22	016.8+07.0	17 56 21.4	-10 57 34.3							1a
PTB23	018.0-02.2	18 31 50.6	-14 15 27.5	18290-1417	1.42	1.77	17.2	182.0	1,3,1,1	1a
PTB24	018.4+05.3	18 05 28.2	-10 20 42.6							1b
PTB25	018.8-01.9	18 32 04.6	-13 26 12.7	18292-1328	1.97	1.14	22.1	301.0	1,3,1,1	1a

^a Independently discovered by Parker et al. 2001b as new PNe (1a) and candidates PNe (1b), and Cappellaro et al. 2001 (2).

A comparison shows a general agreement between the two E_{B-V} calculations within a 3σ error. The signal to noise ratios do not include calibration errors, which are less than 10 percent. The absolute $H\alpha$ fluxes (in units of $\text{erg s}^{-1} \text{cm}^{-2} \text{arcsec}^{-2}$), the exposure time of each individual spectra, the interstellar extinction $c(H\beta)$ with its estimated error and the reddening E_{B-V} (resulting from our observations and SFD maps) are listed in Table 6. Note that due to the low S/N ratio (< 10) of the $H\beta$ line for some of the new PNe

candidates, their accuracy is lower while, the spectrum of PTB6 was taken during a non photometric night, thus its accuracy is even lower and only its relative line fluxes should be taken into account.

5 DISCUSSION

The $\text{H}\alpha + [\text{N II}]$ images as well as the low resolution spectra of the newly discovered PNe candidates were used for a more detailed study. Their relative emission line fluxes confirm that all are photoionized nebulae, according to the diagnostic diagram $\log(\text{H}\alpha/[\text{N II}])$ vs. $\log(\text{H}\alpha/[\text{S II}])$ (García et al. 1991), where they spread well inside the area occupied by PNe (Fig. 3) and their $[\text{S II}]/\text{H}\alpha$ ratio which is in all cases less than 0.3. Note that five of them have very low S/N ratio in their $[\text{N II}]$ and $[\text{S II}]$ emission lines which are not presented in Table 7. However, their $[\text{S II}]/\text{H}\alpha$ is less than 0.2. The angular diameters of the newly discovered PNe have been measured according their optical images ($\text{H}\alpha + [\text{N II}]$), taken with the 1.3 m telescope. It should be noticed that (a) the diameters were defined from the optical outer part of the nebulae, but in some cases it might be slightly larger if a very faint halo exists and (b) that in the case of elliptical shell we present both the major and the minor axes. All diameters are given in Table 6. Thirteen of the new PNe have diameter $\leq 20''$ (Bulge limit – Gathier et al. 1983), 4 are close to this limit ($\leq 25''$), while 8 have diameter $\geq 30''$. The possibility that the latter are evolved and/or their local nature cannot be excluded.

In most cases, a spherical well-defined shell (star-like or ring) was found but nonspherical nebulae (e.g. elliptical) are also present. In particular, 50 percent of the new PNe have a ring-like structure (e.g. PTB15, PTB17), while the rest are divided between faint nebulae with incomplete bright shells (e.g. PTB3, PTB23) and bright compact nebulae (e.g. PTB5, PTB11). The morphological differences could also be attributed to the PN stage of evolution. Compact nebulae in their first stage of expansion look stellar and relatively bright, while large nebulae with faint surface brightness are in their late evolutionary stage. However, three of the new PNe look different. PTB4 is an elongated ring-like nebula probably due to its position angle while, PTB19 is also elongated but with non spherical symmetry at all and PTB7 seems to have a unusual bipolar shape, thus it would be interesting to investigate its morphology further in the future. A morphological type was assigned to the new PNe (Table 6) according to Manchado et al. (2000).

Assuming a temperature of 10^4 $^{\circ}\text{K}$, it is possible to estimate the electron density $n_{[\text{S II}]}$, according to the task “temden” in the nebular package in IRAF for a specific sulfur line ratio ($[\text{S II}] 6716\text{\AA}/[\text{S II}] 6731\text{\AA}$). This task computes the electron density given an electron temperature, of an ionized nebular gas within the 5-level atom approximation (Shaw & Dufour 1995). Furthermore the error of the electron density was calculated through standard error propagation. The electron densities and their associated errors are given in Table 6. Using the observed $[\text{N II}] 6548 + 6584\text{\AA}/[\text{N II}] 5755\text{\AA}$, an estimation for the electron temperature $T_{[\text{N II}]}$ was made whenever possible. In fact only for three of our new PNe (PTB11, PTB17 & PTB24) values close to 10000 $^{\circ}\text{K}$ were found. In those cases where a temperature measurement was not available we assumed a temperature of 10^4 $^{\circ}\text{K}$ (Cuisinier et al. 2000). The high interstellar extinction towards the Galactic bulge as well as the low sensitivity brightness of the new PNe are the main reasons which do not allow to record high quality spectra. This affects mainly the lower intensity lines like $[\text{S II}]$ or HeII , which are faint or even undetectable.

For all PNe of our survey, $\text{H}\alpha$ and $[\text{O III}]$ emission lines could be measured in good conditions and in most cases, $\text{H}\beta$ and $[\text{N II}] 6548$ & 6584 \AA . However, the spectrum for some of the new PNe (e.g. PTB22) has a low signal to noise ratio and only $\text{H}\beta$, $\text{H}\alpha$ and $[\text{O III}]$ are well determined. As can be seen from Fig. 7 emission from $[\text{O III}] 5007$ \AA is present in all observed spectra. Since these PNe are found in a region of significant extinction, shorter wavelengths are more affected than longer wavelengths. In Table 5 we list the measured fluxes in our long-slit spectra corrected for interstellar extinction and is evident that almost all PNe display very strong $[\text{O III}] 5007$ \AA emission relative to $\text{H}\alpha$. It is known that the N/O and He abundances reflect the mass distribution of the progenitor star, with more massive objects having higher N/O and He abundances in comparison with the small-mass objects (Cuisinier et al. 2000). In our case, the abundances in N/O and He generally showed low N/O and He, implying old progenitor stars. The latter suggests that they belong to the Galactic bulge region according to Webster (1988) and Cuisinier et al. (2000) who both showed that the Galactic bulge PNe have old progenitors with low N/O and He abundances. Most of our PNe seem to be of low excitation since they display HeI lines but not HeII . However, there are a few that emit in HeII but not in HeI (like PTB15) which must be highly ionized and this may explain the weakness or absence of the $[\text{N II}] 6548$ & 6584 \AA lines. The excitation classes of our new PNe were studied according the classification criteria of Aller (1956), Feast (1968) and Webster (1975). They are derived basically from the ratios of $[\text{O III}]/\text{H}\beta$, $\text{HeII} 4686\text{\AA}/\text{H}\beta$, $[\text{O II}] 3727\text{\AA}/[\text{O III}] 4959\text{\AA}$ and $\text{HeII} 4686\text{\AA}/\text{HeI} 5876\text{\AA}$. In our case, the $[\text{O III}]/\text{H}\beta$ ratio suggests that our new PNe belong to the medium excitation classes (4–6). However, the absence of the $\text{HeII} 4686\text{\AA}$ and $[\text{O II}] 3727\text{\AA}$ emission lines from our spectra do not allow us to better confine the actual excitation class of each PN.

6 CONCLUSION

We present the first results of a narrowband $[\text{O III}] 5007$ \AA survey for PNe in the Galactic bulge ($l > 0^{\circ}$). Covering 66 percent of our selected region, we detected 90 objects, including 57 known PNe, 8 known PNe candidates and 25 new PNe. $\text{H}\alpha + [\text{N II}]$ images as well as low resolution spectra of the new PNe were taken and confirmed the photoionized nature of the emission. The 70 percent of them have angular sizes $\leq 20''$ – $25''$ while all show $\text{H}\alpha/[\text{O III}] 5007\text{\AA} < 1$. Nine (9) of our new PNe are found to be associated with IRAS sources. They all display low N/O and He abundances implying old progenitor stars, which is one of the characteristics of the Galactic bulge PNe.

ACKNOWLEDGMENTS

The authors would like to thank the referee for his comments and suggestions which helped to clarify, and enhance the scope of this paper. We would also like to thank Q. Parker and A. Acker who provided us the Edinburgh/AAO/Strasbourg Catalogue of Galactic Planetary Nebulae and the First Supplement to the Strasbourg–ESO

Table 5. Line fluxes.

Line (Å)	PTB1	PTB2	PTB3	PTB4	PTB5 ^a	PTB6	PTB7
H β 4861	100.0 (5) ^b	100.0 (11)	100.0 (6)	100.0 (8)	100.0 (39)	100.0 (3)	100.0 (11)
[O III] 4959	317.5 (13)	313.4 (33)	183.8 (12)	213.2 (18)	425.0 (111)	43.1 (2)	172.6 (21)
[O III] 5007	851.3 (32)	928.3 (77)	507.3 (32)	587.0 (47)	1254.2 (184)	405.6 (5)	513.9 (58)
HeII 5411	—	—	—	4.1 (2)	4.7 (9)	—	12.8 (6)
[N II] 5755	—	—	—	—	—	—	—
HeI 5876	17.8 (7)	9.1 (7)	23.2 (8)	16.3 (11)	10.3 (32)	47.1 (4)	17.5 (10)
HeII 6234	—	—	—	—	0.3 (8)	—	—
[N II] 6548	—	—	33.3 (21)	41.0 (29)	1.5 (10)	91.3 (9)	2.7 (4)
H α 6563	285.0 (78)	285.0 (141)	285.0 (104)	285.0 (113)	285.0 (309)	285.0 (24)	285.0 (139)
[N II] 6584	—	—	104.1 (57)	126.0 (74)	4.5 (24)	205.8 (23)	12.1 (9)
HeI 6678	3.6 (8)	1.7 (6)	8.4 (22)	5.2 (7)	3.0 (21)	—	2.6 (2)
[S II] 6716	5.7 (12)	—	9.8 (11)	16.0 (17)	0.9 (7)	21.9 (2)	3.9 (5)
[S II] 6731	6.3 (17)	—	7.4 (9)	12.2 (15)	1.2 (12)	16.8 (2)	2.2 (4)
Line (Å)	PTB8	PTB9	PTB10	PTB11	PTB12	PTB13	PTB14
H β 4861	100.0 (5)	100.0 (23)	100.0 (8)	100.0 (12)	100.0 (21)	100.0 (3)	100.0 (24)
[O III] 4959	327.1 (15)	117.2 (39)	316.6 (27)	305.0 (40)	214.5 (48)	384.9 (7)	345.5 (70)
[O III] 5007	987.5 (41)	357.5 (90)	954.3 (63)	923.4 (87)	629.4 (105)	1573.1 (21)	1040.5 (142)
HeII 5411	—	8.6 (12)	—	—	5.5 (5)	20.0 (2)	—
[N II] 5755	—	—	—	4.6 (2)	—	—	—
HeI 5876	11.0 (4)	29.1 (33)	—	19.3 (16)	10.4 (19)	30.1 (8)	18.3 (31)
HeII 6234	—	—	—	—	—	9.2 (3)	—
[N II] 6548	16.7 (9)	7.7 (16)	—	95.4 (89)	7.4 (11)	—	1.0 (3)
H α 6563	285.0 (71)	285.0 (240)	285.0 (130)	285.0 (175)	285.0 (129)	285.0 (52)	285.0 (258)
[N II] 6584	51.5 (22)	29.9 (48)	—	293.9 (174)	24.7 (26)	—	5.0 (12)
HeI 6678	2.0 (2)	4.9 (25)	—	4.7 (12)	3.3 (7)	—	4.2 (17)
[S II] 6716	7.0 (5)	3.7 (17)	—	65.7 (82)	6.7 (15)	—	0.5 (3)
[S II] 6731	7.9 (6)	4.3 (19)	—	58.7 (77)	5.9 (14)	—	0.5 (1)
Line (Å)	PTB15	PTB16	PTB17 ^a	PTB18 ^a	PTB19	PTB20	PTB21
H β 4861	100.0 (6)	100.0 (6)	100.0 (13)	100.0 (5)	100.0 (26)	100.0 (12)	100.0 (2)
[O III] 4959	235.3 (14)	136.1 (10)	203.4 (29)	204.3 (13)	222.0 (56)	471.0 (47)	431.1 (7)
[O III] 5007	653.1 (38)	462.8 (29)	604.5 (71)	600.4 (36)	646.7 (110)	1412.3 (90)	949.6 (18)
HeII 5411	11.6 (3)	10.2 (3)	—	5.6 (9)	—	4.9 (5)	—
[N II] 5755	—	—	4.0 (4)	—	—	—	—
HeI 5876	—	16.6 (7)	22.4 (18)	12.9 (8)	16.3 (41)	16.6 (16)	—
HeII 6234	2.4 (5)	—	—	—	—	—	—
[N II] 6548	—	2.6 (2)	103.6 (57)	88.4 (19)	2.6 (12)	9.2 (26)	63.0 (6)
H α 6563	285.0 (82)	285.0 (83)	285.0 (94)	285.0 (44)	285.0 (198)	285.0 (192)	285.0 (22)
[N II] 6584	—	7.8 (6)	323.3 (77)	270.5 (36)	8.2 (30)	32.7 (22)	172.7 (14)
HeI 6678	—	10.9 (3)	5.0 (9)	6.6 (2)	4.4 (28)	3.3 (14)	10.9 (3)
[S II] 6716	—	7.4 (2)	36.9 (28)	41.1 (16)	1.1 (9)	1.2 (9)	40.1 (5)
[S II] 6731	—	4.5 (1)	29.1 (23)	33.2 (12)	1.4 (11)	2.5 (11)	27.1 (4)
Line (Å)	PTB22	PTB23 ^a	PTB24	PTB25 ^a			
H β 4861	100.0 (4)	100.0 (28)	100.0 (7)	100.0 (19)			
[O III] 4959	380.7 (13)	397.4 (88)	260.7 (19)	231.4 (47)			
[O III] 5007	1147.6 (38)	1152.2 (172)	838.4 (49)	671.6 (111)			
HeII 5411	—	9.6 (8)	—	8.1 (8)			
[N II] 5755	—	—	3.3 (9)	—			
HeI 5876	—	2.3 (4)	14.0 (8)	3.0 (5)			
HeII 6234	—	—	—	1.2 (5)			
[N II] 6548	—	2.0 (7)	76.9 (36)	1.9 (5)			
H α 6563	285.0 (45)	285.0 (147)	285.0 (97)	285.0 (207)			
[N II] 6584	—	5.7 (14)	233.9 (82)	7.0 (14)			
HeI 6678	—	1.5 (3)	3.2 (3)	—			
[S II] 6716	—	3.1 (10)	40.4 (27)	3.3 (8)			
[S II] 6731	—	3.5 (8)	29.2 (20)	3.1 (7)			

^a Listed fluxes are a signal to noise weighted average of the individual fluxes

^b Numbers in parentheses represent the signal to noise ratio of the line fluxes, measured at the center of the corresponding emission line profile.

 All fluxes normalized to $F(H\beta)=100$ and they are corrected for interstellar extinction.

Table 6. Exposure time and basic physical parameters.

Object	Exp. time	Diameter ¹	M.Type ²	F(H α) ³	c(H β) ⁴	$\sigma_{c(H\beta)}^5$	$E_{B-V(OBS)}^6$	$\sigma_{E_{B-V}}^7$	$E_{B-V(SFD)}^8$	$n_{[S\,II]}^9$	$\sigma_{n_{[S\,II]}}^{10}$
PTB1	3600 ¹¹ (1) ¹²	33.0	R	3.9	2.25	0.26	1.55	0.18	1.26	0.93	0.33
PTB2	3600 (1)	15.0	B	11.1	1.38	0.12	0.95	0.08	1.18	<0.07	—
PTB3	3600 (1)	23.0	R	4.52	1.78	0.21	1.23	0.15	0.92	0.09	0.08
PTB4	2700 (1)	17.0×8.0	E	9.0	1.70	0.15	1.17	0.10	1.09	0.12	0.10
PTB5	4800 (2)	10.0	R	40.7	1.20	0.02	0.83	0.01	0.84	1.88	0.81
PTB6	2700 (1)	20.0	E	1.2	1.42	0.50	0.98	0.35	0.93	<0.07	—
PTB7	3600 (1)	25.0×10.0	B	4.6	0.85	0.11	0.59	0.08	0.64	<0.07	—
PTB8	2500 (1)	19.0	R	5.6	1.73	0.25	1.19	0.17	1.10	0.95	0.88
PTB9	3600 (1)	18.0×16.0	E	5.9	1.25	0.05	0.86	0.04	0.92	1.10	0.31
PTB10	3600 (1)	10.0×8.0	E	7.2	1.84	0.16	1.27	0.11	0.94	<0.07	—
PTB11	3600 (1)	10.5	R	17.6	1.92	0.11	1.32	0.07	1.30	0.36	0.03
PTB12	3600 (1)	17.0×14.0	E	15.7	1.19	0.06	0.82	0.04	0.90	0.34	0.18
PTB13	3600 (1)	11.0	R	4.3	2.74	0.48	1.89	0.33	1.05	<0.07	—
PTB14	3600 (1)	9.0	R	32.5	1.58	0.05	1.09	0.03	0.92	0.28	0.27
PTB15	3600 (1)	33.0	R	4.2	1.58	0.21	1.09	0.15	1.12	<0.07	—
PTB16	3600 (1)	24.5	R	3.3	1.08	0.22	0.74	0.15	0.51	<0.07	—
PTB17	5400 (2)	32.0	R	9.0	1.35	0.07	0.93	0.05	0.92	0.16	0.06
PTB18	4800 (2)	38.0	R	2.2	0.63	0.19	0.44	0.13	0.51	0.19	0.11
PTB19	3600 (1)	17×20.0	E	40.1	1.93	0.05	1.33	0.03	1.31	1.71	0.72
PTB20	2700 (1)	10.0	R	7.8	1.94	0.11	1.34	0.08	1.25	20.74	12.0
PTB21	3600 (1)	69.0	R	0.6	0.94	0.48	0.65	0.33	1.07	<0.07	—
PTB22	2700 (1)	34.5	R	2.1	1.48	0.34	1.02	0.23	0.98	<0.07	—
PTB23	4800 (2)	46.0×38.0	E	24.8	0.62	0.13	0.43	0.09	1.69	2.05	0.60
PTB24	2700 (1)	16.0	R	4.3	1.55	0.19	1.07	0.13	1.13	<0.07	—
PTB25	5400 (2)	40.0	R	9.2	0.99	0.15	0.69	0.10	1.44	0.47	0.32

¹ Optical diameters in arcsec.² Morphological classification according to Manchado et al. (2000), where R(=round), E (=elliptical) and B (=bipolar).³ Absolute H α flux in units of 10^{-16} erg s $^{-1}$ cm $^{-2}$ arcsec $^{-2}$.⁴ Logarithmic extinction at H β (see Sect. 4.2).⁵ 1 σ error on the logarithmic extinction.⁶ Observed Reddening (see Sect. 4.2).⁷ Error on the observed reddening.⁸ Reddening according the maps of Schlegel et al. 1998 (see Sect. 4.2).⁹ Electron density in units of 10^3 cm $^{-3}$ (see Sect. 5).¹⁰ Error on the electron density.¹¹ Total exposure time in sec.¹² Number of individual exposures.

Catalogue of Galactic Planetary Nebulae, respectively and E. Semkov, G. Paterakis, A. Kougentakis and A. Strigachev for their assistance and help during these observations. Skianakas Observatory is a collaborative project of the University of Crete, the Foundation for Research and Technology-Hellas, and the Max-Planck-Institut für extraterrestrische Physik.

REFERENCES

Acker A., Cuisinier F., Stenholm B. & Terzan A., 1992a, A&A, 264, 217

Acker A., Ochsenbein F., Stenholm B., Tylenda R., Marcout J. & Schönh C., 1992b, in the Strasbourg-ESO Catalogue of Galactic Planetary Nebulae, Parts 1 and 2 (Strasbourg: ESO)

Acker A., Marcout J., Ochsenbein F., Beaulieu S., Garcia-Lario P. & Jacoby G., 1996, First Supplement to the Strasbourg-ESO Catalogue of Galactic Planetary Nebulae (Strasbourg: Obs. Strasbourg)

Aller L. H., 1956, Gaseous Nebulae (New York: Wiley)

Beaulieu S. F., Dopita M. A. & Freeman K. C., 1999, ApJ, 515, 610

Beaulieu S. F., Freeman K. C., Kalnajs A. J., Saha P. & Zhao H., 2000, AJ, 120, 855

Boumis P. & Papamastorakis J., 2002, proceedings of the 5th Hellenic Astronomical Society Conference, held in Fodele Crete, Greece, 20-22 September 2001, in press

Boumis P. et al., 2003, MNRAS, in preparation (paper II)

Cappellaro E., Sabbadin F., Benetti S. & Turatto M., 2001, A&A, 377, 1035

Ciardullo R., Jacoby G. H., Ford H. C. & Neil J. D., 1989, ApJ, 339, 53

Condon J. J., Kaplan D. L. & Terzian Y., 1999, ApJS, 123, 219

Cuisinier F., Maciel W. J., Köppen J., Acker A. & Stenholm B., 2000, A&A, 353, 543

Durand S., Acker A. & Zijlstra A., 1998, A&AS, 132, 13

Egan, M. P., et al., 1999, in Astrophysics with Infrared Surveys, A Prelude to SIRTF, ed. M. D. Bicay, R. M. Cutri, & B. F. Madore, ASP Conf. Ser., 177, 404

Escudero A. V. & Costa R. D. D., 2001, A&A, 380, 300

Feast M. W., 1987, The Galaxy, eds. Gilmore G. & Carswell B. (Reidel, Dordrecht), 1

Feldmeier J. J., Ciardullo R. & Jacoby G. H., 1997, *ApJ*, 479, 231
 Fitzpatrick E. L., 1999, *PASP*, 111, 63
 García-Lario P., Manchado A., Riera A., Mampaso A. & Pottasch S. R., 1991, *A&A*, 249, 223
 Gathier R., Pottasch S. R., Goss W. W. & van Gorkom J. H., 1983, *A&A*, 128, 325
 Hamuy M., Walker A. R., Suntzeff N. B., Gigoux P., Heathcote S. R. & Phillips M. M., 1992, *PASP*, 104, 533
 Hamuy M., Suntzeff N. B., Heathcote S. R., Walker A. R., Gigoux P. & Phillips M. M., 1994, *PASP*, 106, 566
 Hui X., Ford H. C., Ciardullo R. & Jacoby G. H., 1993, *ApJ*, 414, 463
 IRAS Point Source Catalog, Version 2, 1988, Joint IRAS Science Working Group (Washington, DC: GPO)
 Jacoby G. H., Ciardullo R., Ford H. C. & Booth J., 1990, *ApJ*, 365, 471
 Kimeswenger S., Kienel C. & Widauer H., 1997, *Ap&SS*, 210, 105
 Kimeswenger S., 2001, *Rev.Mex.A.A.*, 37, 115
 Kinman T. D., Feast M. W. & Lasker B. M., 1988, *AJ*, 95, 804
 Kohoutek L., 1997, *AN*, 318, 35
 Kohoutek L., 2001, *A&A*, 378, 843
 Köppen J. & Vergely J.-L., 1998, *MNRAS*, 299, 567
 Lasker B. M., Russel J. N. & Jenkner H., 1999, in the HST Guide Star Catalog, version 1.1-ACT, The Association of Universities for Research in Astronomy, Inc
 Lauberts A., 1982, The ESO/Uppsala Survey of the ESO (B) Atlas, European Southern Observatory
 2MASS Point Source Catalog, 2000, NASA/IPAC Infrared Science Archive, Jet Propulsion Laboratory (California Institute of Technology)
 Manchado A., Guerrero M. A., Stanghellini L. & Serra-Ricart M., 1996, in the IAC Morphological Catalog of Northern Galactic Planetary Nebulae (IAC)
 Manchado A., Villaver E., Stanghellini L. & Guerrero M., 2000, in ASP Conf. Ser. 199, Asymmetrical Planetary Nebulae II: From Origins to Microstructures, eds. Kastner et al., 17
 Minniti D., Olszewski E. W., Liebert J., White S. D. M., Hill J. M. & Irwin M. J., 1995, *MNRAS*, 277, 1293
 Minniti D., 1996a, *ApJ*, 459, 175
 Minniti D., 1996b, *ApJ*, 459, 579
 Moreno H., Lasker B. M., Gutierrez-Moreno A. & Torres C., 1988, *PASP*, 100, 604
 Morison H. L. & Harding P., 1993, *PASP*, 105, 977
 Osterbrock D. E., 1989, *Astrophysics of Gaseous Nebulae and Active Galactic Nuclei*, vol. 9 (University Science Books)
 Parker Q. A., Hartley M., Russel D., Acker A., Morgan D., Beaulieu S., Morris R., Phillips S. & Cohen M., 2001a, IAU Symposium No. 209, Planetary Nebulae: Their Evolution and Role in the Universe (Canberra, Australia, November 19 - 23 2001), in press
 Parker Q. A., Hartley M., Russel D., Acker A., Ochsenbein F., Morgan D., Beaulieu S., Morris R., Marcout J., Cohen M. & Phillips S., 2001b, in the Edinburgh/AAO/Strasbourg Catalogue of Galactic Planetary Nebulae, Preliminary version 1.0 November 2001
 Pottasch S. R., Bignell C., Olling R. & Zijlstra A. A., 1988, *A&A*, 205, 248
 Rataj M. A., 1990, PhD thesis, Univ. Groningen
 Sevenster M. N., 1999, *MNRAS*, 310, 629
 Schlegel D. J., Finkbeiner D. P. & Davis M., 1998, *ApJ*, 500, 525
 Schneider S. E. & Buckley D., 1996, *ApJ*, 459, 606
 Seaton M. J., 1979, *MNRAS*, 187, L73
 Shaw R. A. & Dufour R. J., 1995, *PASP*, 107, 896
 van de Steene G. C., 1995, PhD thesis, Univ. Groningen
 van de Steene G. C., & Jacoby G. H., 2001, *A&A*, 373, 536
 van Hoof P. A. M. & van de Steene G. C., 1999, *308*, 623
 Walker A. R. & Terndrup D. M., 1991, *ApJ*, 378, 119
 Webster L., 1975, *MNRAS*, 173, 437
 Webster L., 1988, *MNRAS*, 230, 377
 Weiland J. L., et al., 1993, in AIP Conf. Proc. 278, Back to the Galaxy, eds. Holt S.S. & Verter F. (New York: AIP), 137
 Whitelock P., 1993, in IAU Symp. 153, Galactic Bulges, eds. De Jonghe H. & Habing H. J. (Dordrecht: Kluwer), 39
 Whitelock P., Menzies J., Feast M., Marang F., Carter B., Roberts G., Catchpole R. & Chapman J., 1994, *MNRAS*, 267, 711
 Xilouris K. M., Papamastorakis J., Sokolov N., Paleologou E. & Reich W., 1994, *A&A*, 290, 639
 Zijlstra A. A. & Pottasch S. R., 1991, *A&A*, 243, 478

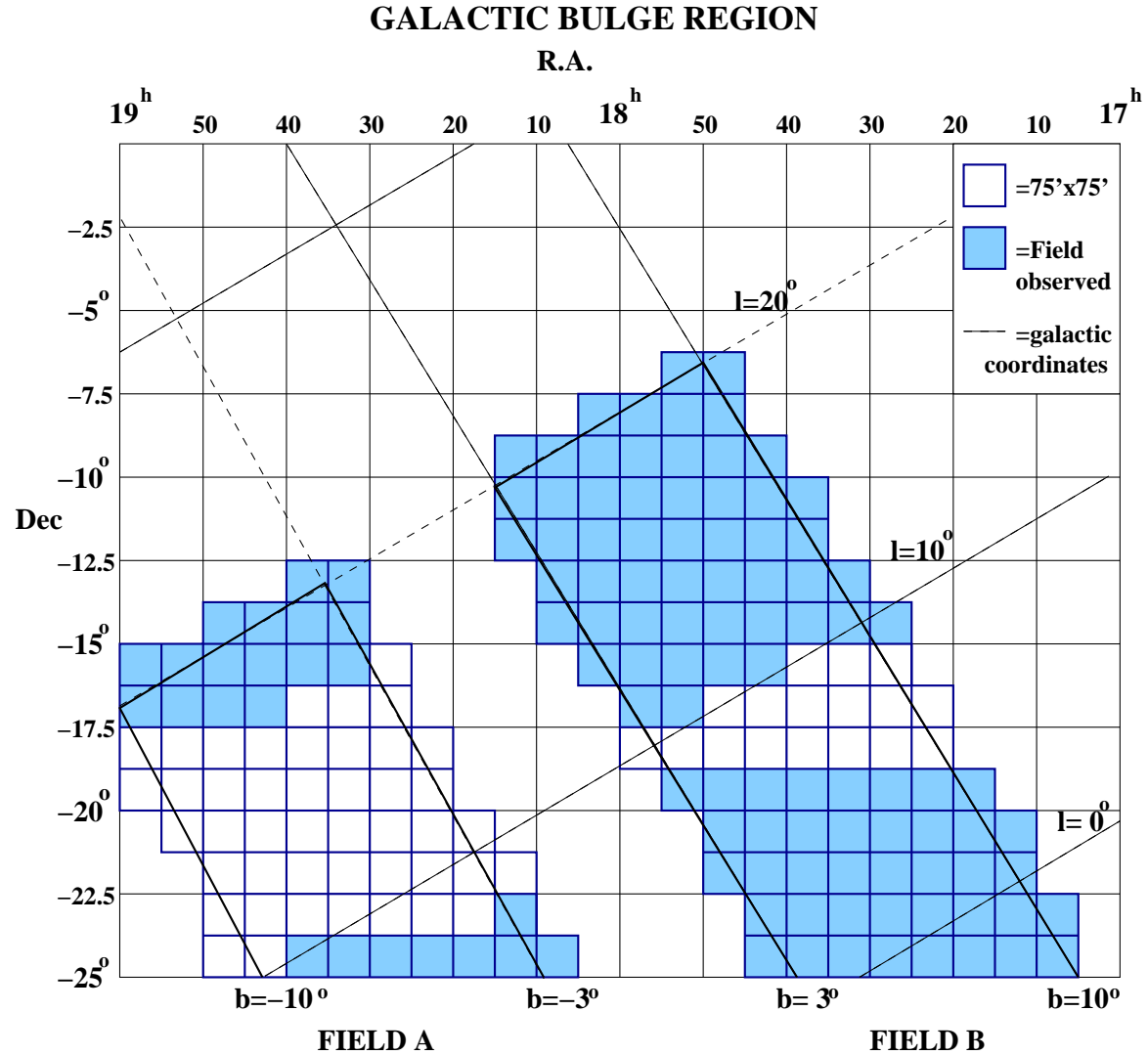


Figure 1. Optical imaging survey grid in equatorial coordinates. Galactic coordinates are also included (dash lines) to permit an accurate drawing of the selected Bulge region (bold solid lines). The filled and open rectangles represent the observed and not yet observed fields in the year 2000, respectively.

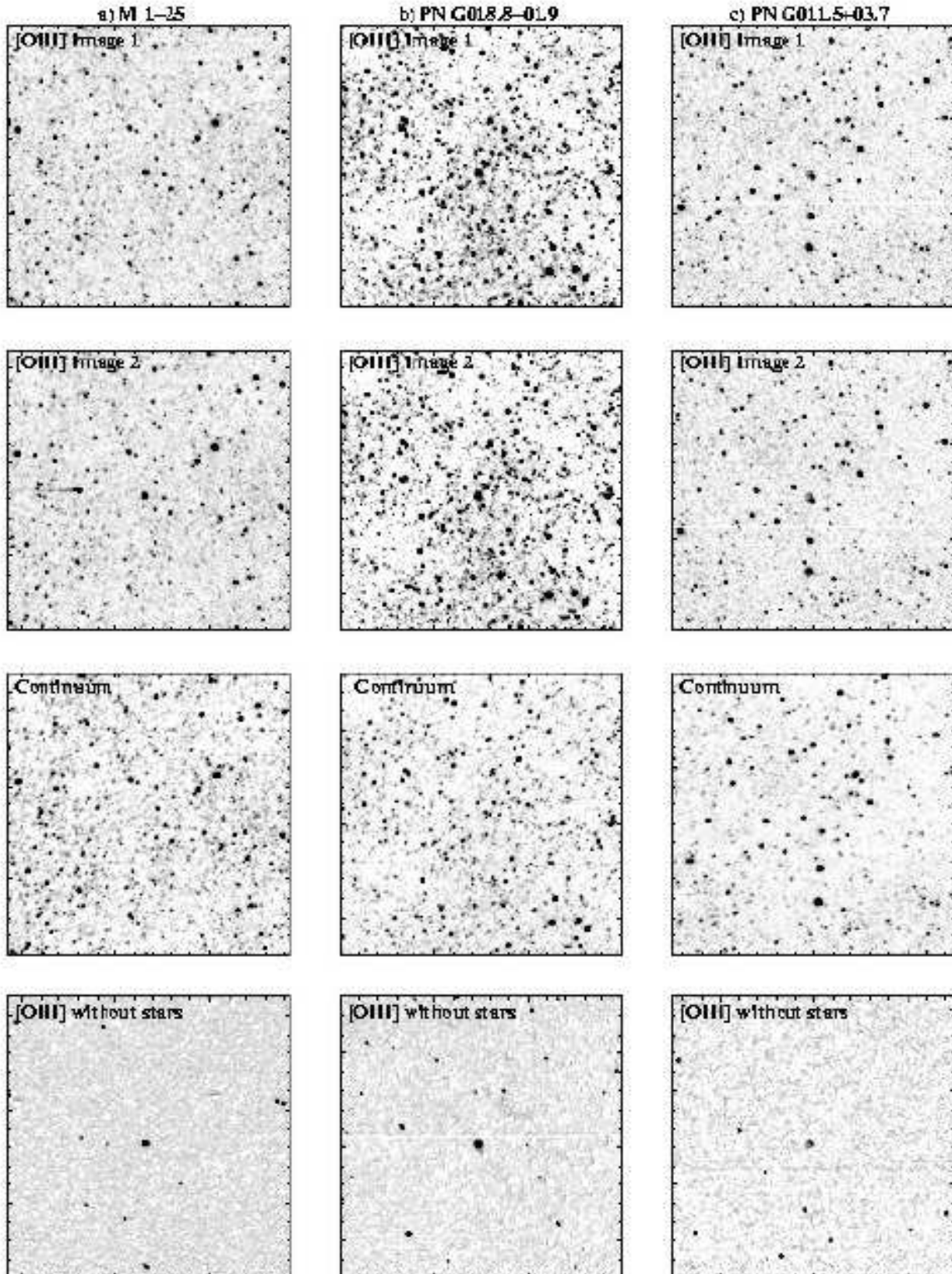


Figure 2. Examples of images ($20'$ on both sides each) for three different objects which show our survey's typical discoveries. The first set of images (a) is a known PN which was found and presented for comparison reasons; the other two sets (b) and (c) are new discoveries. Note that the remaining black dots in the last image of each set (except the PNe) are cosmic rays which did not remove with the continuum subtraction. North is at the top, East to the left.

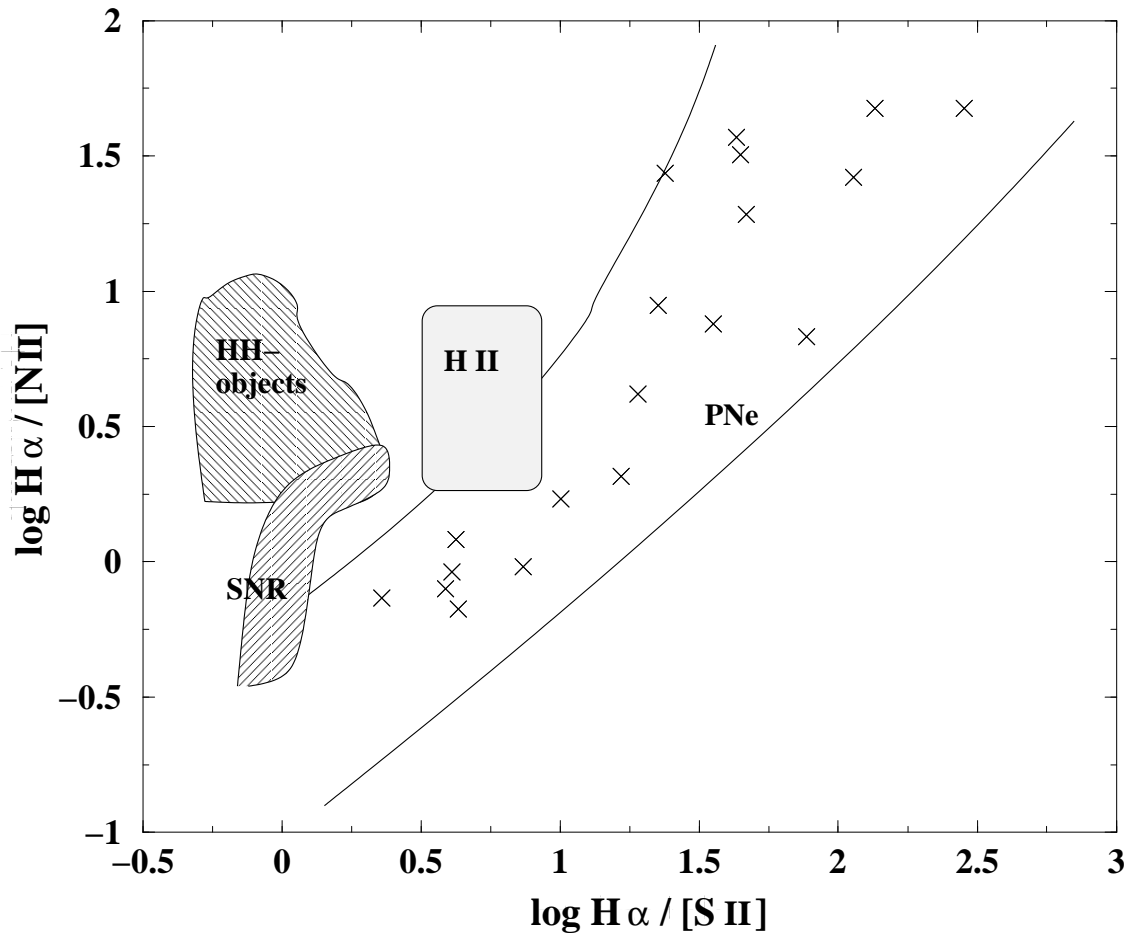


Figure 3. Diagnostic diagram (Garcia et al. 1991), where the positions of the new PNe are shown with a cross (X).

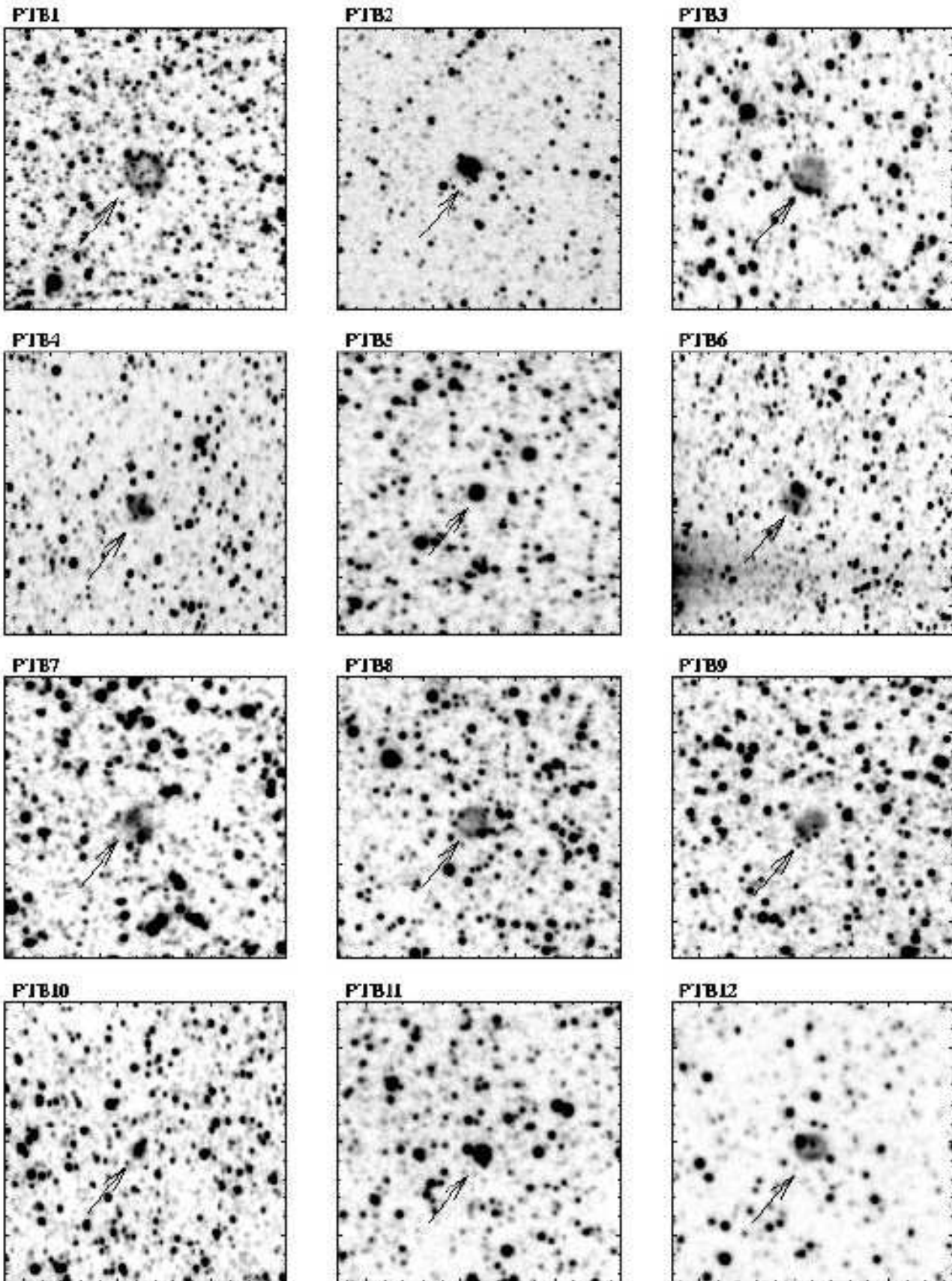


Figure 4. $\text{H}\alpha + [\text{N II}]$ images of all the new PNe taken with the 1.3 m telescope. Black arrows indicate their position at the centre of each image. The latter, have a size of $150''$ on both sides. North is at the top, East to the left.

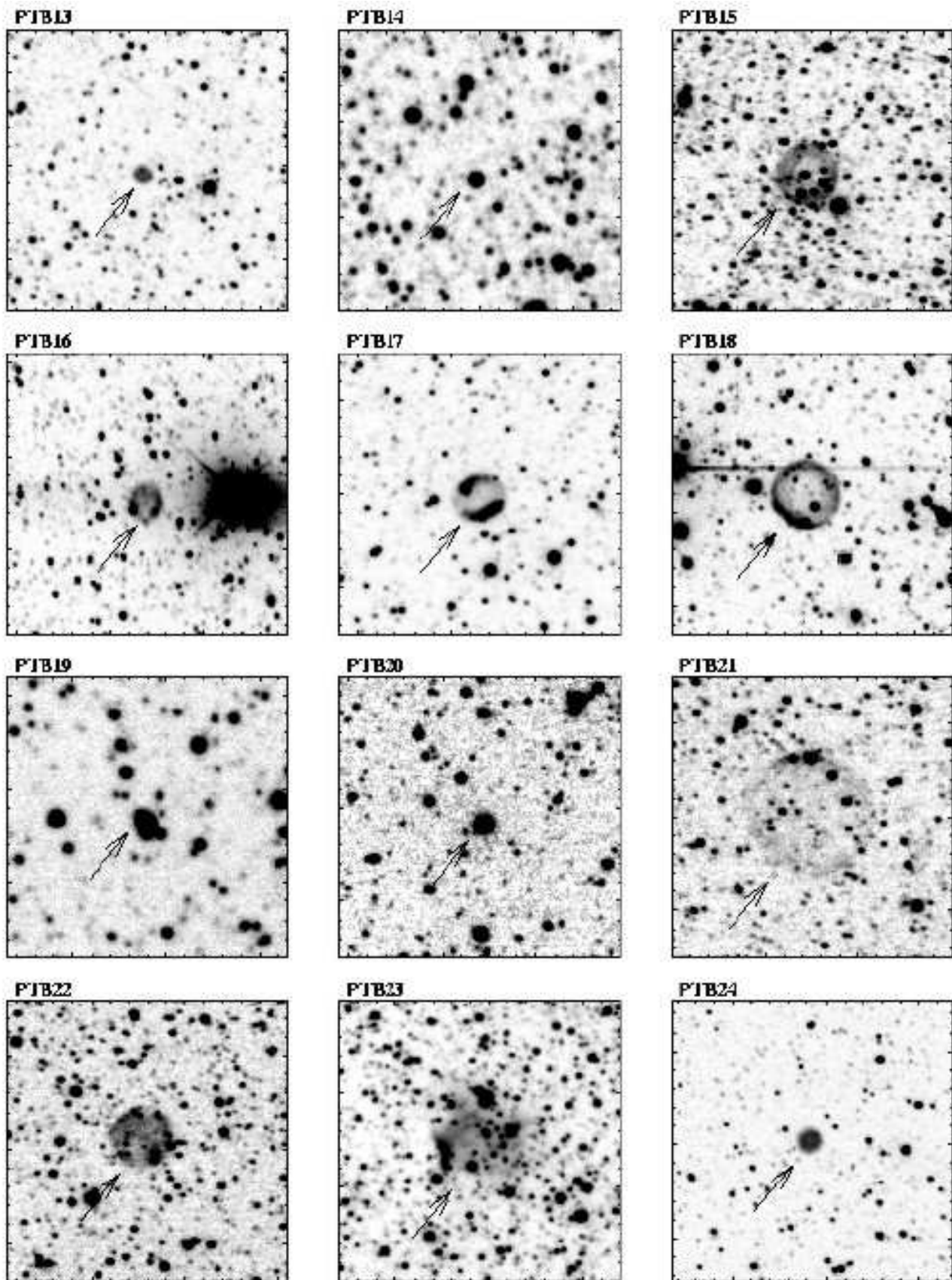


Figure 5. Fig. 4 (Continued)

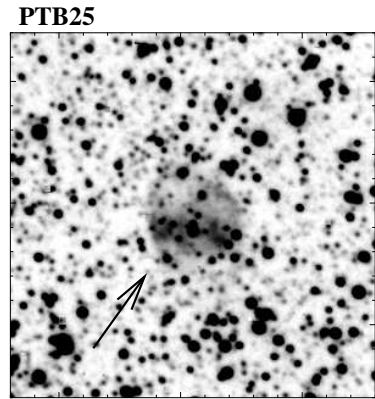


Figure 6. Fig. 4 (Continued)

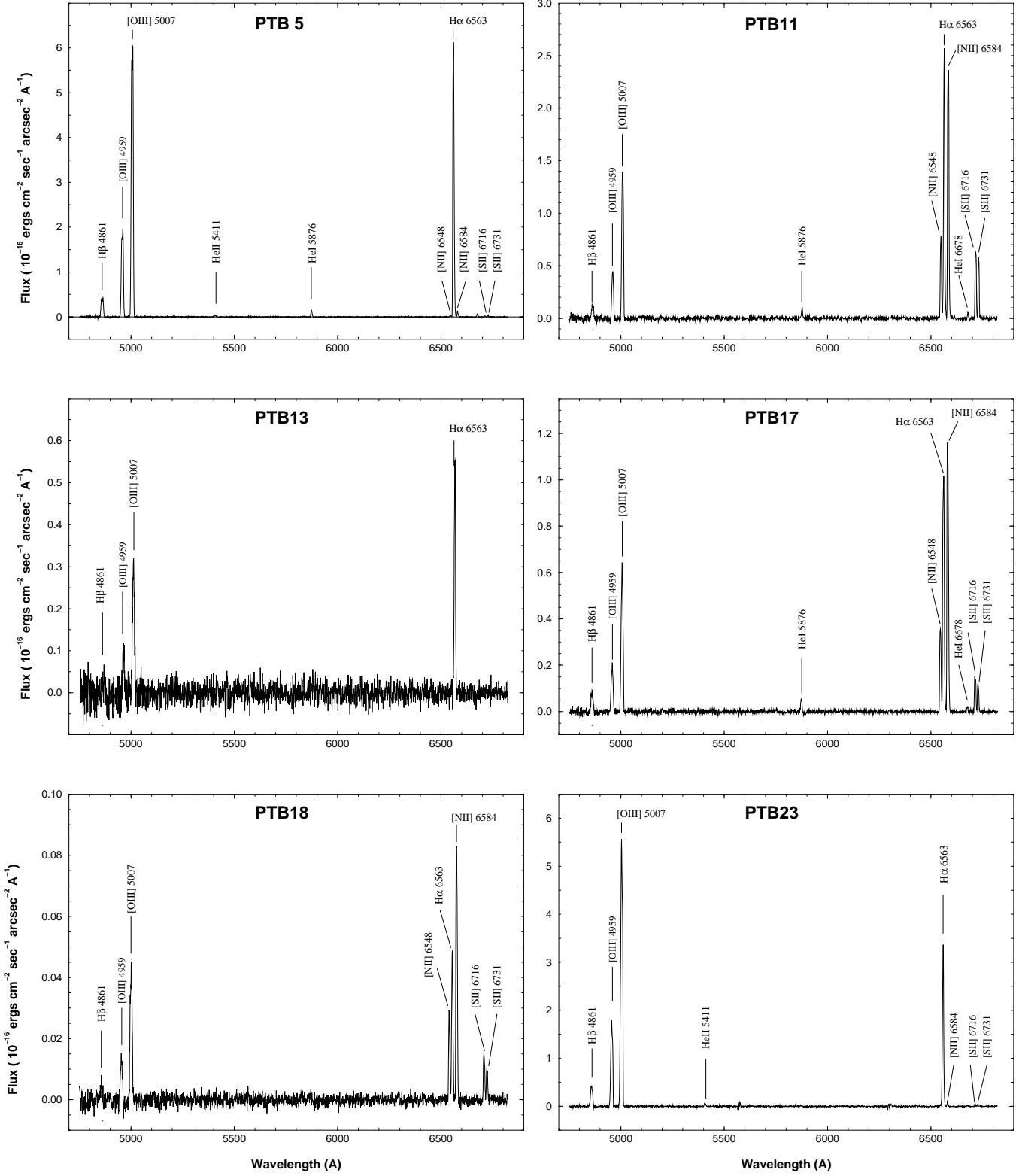


Figure 7. Typical observed spectra of our new PNe taken with the 1.3 m telescope. They cover the range of 4750Å to 6815Å and the emission line fluxes (in units of 10^{-16} erg s $^{-1}$ cm $^{-2}$ arcsec $^{-2}$ Å $^{-1}$) are corrected for atmospheric extinction. Line fluxes corrected for interstellar extinction are given in Table 5.